Tailoring the Bandgap and magnetic properties by Bismuth substitution in Neodymium Chromite

Venkateswara rao Mannepalli, Saj Mohan M M and R. Ranjith[*]

Department of Materials Science & Metallurgical Engineering,
Indian Institute of Technology Hyderabad,
Kandi, Sanga reddy-502285, Telangana, India.

Abstract

The intrinsic distortions present in rare earth ortho chromites ($RCrO_3$) observed from lanthanum to lutetium (in R-site) can influence the magnetic properties like Neel Transition and weak ferromagnetic coupling. A non-magnetic cation with similar ionic radius would be a suitable candidate to engineer the inherent distortions of particular orthochromite. In this study Bismuth (Bi^{3+}) with a $6s^2$ lone pair was chosen to substitute in Neodymium (Nd^{3+}) site of $NdCrO_3$ (NCO) to tailor the intrinsic structural distortions. The variation of optical absorption edge evidently suggests that Bi ($6s^2$) substituted in the magnetic rare earth Nd^{+3} influences the Cr-O overlap integral. The interaction of Bi cation with oxygen bonds influences the structural distortions through Cr-O polyhedra which are evident from Raman scattering studies. The observed structural and magnetic properties of similar ionic radius of Bi^{3+} in Nd^{3+} reveals that intrinsic structural distortions are interrelated to enhanced weak ferromagnetic component and change in Neel and spin reorientation temperatures in our compounds. In addition a reduction in the optical band gap of NCO from 3.1 eV to 2.6 eV was observed.

Key words: Raman Spectroscopy, Magnetic Properties and Optical Band gap

[*] *corresponding author* : ranjith@iith.ac.in

1. INTRODUCTION

Orthochromites, $RCrO_3$, (R- Rare earth) are interesting family of compounds due to intriguing physical properties and their complex magnetic interactions. These compounds has received wide attention aiming at versatile applications like solid oxide fuel cells [1,2], Negative temperature coefficient (NTC) thermistors [3], Multiferroic applications [4-7] etc. The intriguing ferroelectric nature of magnetic rare earth ortho chromites $RCrO_3$ (R= Sm, Gd, Er, Tb and Tm) is expected to arise by the local symmetry breaking due to the interaction between magnetic rare earth ion and weak ferromagnetic Cr^{3+} ions leads at magnetic ordering temperatures[4]. Thus the short range polar order in chromates is due to local symmetry present in the samples [8]. In addition, the nonmagnetic nature of yttrium can also induce polar nature in $YCrO_3$ due to inherent distortions present in system [6,9,10]. On the other hand $RCrO_3$ show extremely rich magnetic properties due to interaction between R^{3+}-R^{3+}, R^{3+}-Cr^{3+} and Cr^{3+}-Cr^{3+} ions leading to various types of magnetic ordering at different temperatures. The Cr^{3+} moments in all rare earth orthochromite pervoskites exhibits G-type antiferromagnetic structure at Neel temperatures (T_N) ranging from 115 to 289K and also possess weak ferromagnetic order below T_N [11,12,13]. Presence of magnetic moment at rare earth site in ortho chromites enhances the magnetization due to Cr^{3+} sublattice polarize R^{3+} rare earth ions[14] which results into another transition at low temperatures called spin reorientation temperature T_{SRPT}. Due to the interaction of R^{3+}-Cr^{3+} (R= Gd, Nd, Ho, Er, Tm) in orthochromites the T_{SRPT} varies from 6.5 to 35K. [15,16,17,18] The rare earth ordering due to weak interactions among R^{3+}-R^{3+} can be observed at very low temperatures and in some compounds like $HoCrO_3$ and $PrCrO_3$ the rare earth ordering is not at all observed with in the measured temperature range [13]. Few magnetic rare earth chromites also show magnetization reversal properties due to rare earth moments are aligned antiparallel to the chromium magnetic moments [16,19]. The strong among these interactions are Cr^{3+}-Cr^{3+} responsible for antiferromagnetic ordering in chromites and it is greatly influenced by the rare earth ionic radius. A monotonic decrease of T_N is observed in series of orthochromites with decreasing of ionic radius of rare earth and mixed orthochromites [13,14]. The observed weak ferromagnetic nature below T_N in these chromites is due to canting of the Cr^{3+} system which arises from the Dzyaloshinsky-Moriya exchange interaction[20]. When compared the Neel transition temperature dependence of orthoferrite with the ortho chromites (isostructural and non JahnTeller active ions) with the variation of ionic size of rare earth ion, the former

depends on Fe^{3+}-O-Fe^{3+} bond angle [21] whereas the latter dependence on Cr^{3+}-O-Cr^{3+} bond angle is overall 30% of T_N [22]. Thus additional intrinsic structural distortions which leads to involvement of overlapping *t* and *e* orbitals of Cr^{+3} in orthochromites along with the bond angle dependence in chromites can explain the observe T_N variation with ionic sizes[22]. This can be understood from the simple picture of octahedra units built by pervoskite oxides. When a transition metal is surrounded by six oxide ions in a regular octahedral arrangement, *3d* orbitals of Cr ($3d^3$) splits into two groups, a lower triplet, t_{2g} *or t* and an upper doublet e_g *or e*. The physical basis for this splitting is simply the electrostatic repulsion between the *d* electrons and the surrounding negative oxygen ions where the e_g orbitals point directly at these ions and the t_{2g} orbitals point in between the ions. Although this simple picture does not take covalent bonding into account; its inclusion does not affect the fundamental result [23]. After involving the covalent bonding, it leads to exactly same kind of splitting into a lower nonbonding t_{2g} orbital and an upper antibonding e_g orbital with difference in magnitude of the energy separation between the two orbitals. Thus the inclusion of mixed ionic and covalent character of metal to oxygen bonding in metal ion influences the T_N. However, in chromites, size or ionic radius of rare earth cations (Lu-La) plays important roles on the structural distortions of $RCrO_3$ which makes the octahedra are linked in canting position with each other[22,24]. These structural distortions indeed involve the change in bond angles which further leads to inherent bond overlap of t_{2g} (filled) and e_g (unfilled) orbitals of Chromium with oxygen and observed changes in T_N. Thus t_{2g}-e_g hybridization is inevitable with the change of bond angle in chromites whereas this hybridization on Fe^{3+}(t^3e^2) (i.e. t^3-*O*-t^3 and e^2-*O*-e^2) did not bring any change of T_N in orthoferrites. The observed weak ferromagnetic coupling in these chromates (Cr^{3+}:t^3e^0) can be understood by the super exchange interaction between two adjacent transition metal ions is delivered by a virtual charge transfer [22] i.e. t_{2g}^3-*O*-e_g^0. Thus understanding on orthorhombic pervoskites that possess intrinsic structural distortions in addition to the cooperative octahedral-site BO_6 (B=Fe, Cr, Mn) rotations are essential elements to interpret magnetic properties in these systems [25]. In this study we attempt to tune the inherent structural distortions which can in turn affect the magnetic properties of $RCrO_3$ especially $NdCrO_3$. Structural [26], Magnetic susceptibility [27], Neutron studies [12,28] and specific heat properties [29] investigations performed on $NdCrO_3$ and also limited number of studies such as $Nd_{1-x}Eu_xCrO_3$ [17], $Nd_{1-x}La_xCrO_3$ [30], $Nd_{1-x}Sr_xCrO_3$ [28] to understand the altered interactions among Nd and Cr in $NdCrO_3$. These studies reveal that the effect

of substitution of higher ionic radius or magnetic rare earth ions in Nd-site either dilutes the Nd-Cr coupling or decrease of structural distortions due to increase of bond angle further leads to increase of T_N. Inorder to understand the inherent structural distortions and its relation to magnetic properties, a nonmagnetic and similar radius of Nd^{3+} is suitable candidate for the study. At present we have chosen an element other than rare earth, nonmagnetic Bismuth cation (r_{Bi3+}=1.11Å), which is prone to introduce local *structural distortion* due to the presence of stereo chemically active $6s^2$ lone pair electron [31] and profoundly influence the magnetic properties. Unlike the electron configuration of Nd^{3+} (r_{Nd3+}=1.109Å) ions ($4f^3$), the outermost shell of Bi^{3+} ($6s^2$) is fully occupied. To the best of our knowledge structural distortions interrelated magnetic and optical properties of Bi^{3+} in Nd^{3+} of $NdCrO_3$ have not been reported due to high pressure synthesis [32] required for Bi-based chromates. The substitution of Bi^{3+} in $NdCrO_3$ of its own is challenging and not many efforts have been carried out in orthochromites. In this study $Nd_{1-x}Bi_xCrO_3$ (NBiCO) with varying Bi content was successfully synthesized by Sol-gel route upto 15 at% Bi substituted at Nd^{3+} site.

2. MATERIALS AND METHODS

$Nd_{1-x}Bi_xCrO_3$ (x=0, 0.05, 0.1, 0.15 at %) (NBiCO) was synthesized by the Sol-gel method using the nitrates of Neodymium, Bismuth and Chromium. Nitrates of Neodymium and Bismuth are prepared from the oxides dissolved in nitric acid whereas chromium nitrate ($Cr(NO_3)_3.9H_2O$) is obtained from the sigma Aldrich (99% pure). The Nitrates of all cations are homogeneously mixed with simultaneous addition of citric acid (chelating agent) and ethylene glycol (gelating agent). The obtained solution was dried at 393K for 2days and then heat treated to evaporate the nitrates. The extracted powder was calcined at 1123K for 4 hrs. Calcined powders were pelletized by adding freshly prepared polyvinyl alcohol solution as binder and sintered at 1373K for 10hrs in closed environment, inorder to minimize the loss of Bismuth. Structural analysis was performed through X-ray powder diffraction (XRD) studies at room temperature (RT~303K) (Panalytical X'pert Pro, Cu K_α radiation). Rietveld refinement was performed on the powder diffraction data by using '*full proof*' software [33]. The phonon modes of all the synthesized compounds was studied using a Laser Micro Raman spectrometer (Bruker, Senterra) with an excitation source of 532nm at RT. Magnetic measurements are carried out by Physical Property Measurement System (PPMS)

Dynacool (Quantum design, USA) with magnetic fields varied from -5T to +5T and temperature sweep from 5-300K. The optical studies were done by using UV-Vis Spectrometer lambda 1050 make Perkin Elmer

3. RESULTS AND DISCUSSION

3.1 Structural diffraction patterns

Rietveld refinements of NBiCO were carried out using the orthorhombic crystal system with the centrosymmetric *Pnma* space group, which shows good agreement between the observed and calculated diffraction patterns shown as difference (Y_{obs}-Y_{cal}) plot given at the bottom ensures a reliable fit of the experimental data. The bars represent in the Fig 1 are Bragg diffraction positions and the reasonable reliability parameters such as low R-factors and $\chi 2$ values indicate the authencity of the refinement. The background was refined with 6^{th} order polynomial function and Pseudo-Voight is used as peak shape profile to refine the patterns. The diffraction patterns revealed that x= 0.15 refined with the single phase orthorhombic *Pnma* symmetry along with minor amount (< 2%) of Bi_2O_3 (nonmagnetic) impurity .The observations suggests that the solubility of Bismuth (Bi) in Nd site is lower than 15 at. % through our sol-gel processing technique. Single phase of NBiCO and the minimal change of lattice parameters (Table 1) show that the similar ionic radius of Bismuth occupies the Neodymium site. The observed average change in bond angles from 154º to 152º upto 10at% through our XRD patterns. The average change in bond lengths such as Cr-O1 (1.984 to 1.973Å), Nd-O1 (3.14 to 3.2 Å), Cr-O2 (1.97 to 1.95) and Nd-O2 (2.72 to 2.49 Å) indicates a *global* structure orthorhombic (*Pnma)* throughout the composition range. Even though the XRD structure remains the same but the difference of electronic configuration and sterochemical activity of 'Bi' in 'Nd' site is expected to affect the *local* structural distortions such as CrO_6 rotations has its impact on physical properties.

3.2 Phonon Studies

Raman spectroscopy is a versatile technique to investigate the lattice dynamics of pervoskites and also reveal the local structural distortions due to CrO_6 rotations or displacement of cations in a unit cell. The irreducible representation of the Raman modes [34] for the pervoskite orthorhombic pervoskite structure at the center of the brillioun zone is given by equation (1).

$$\Gamma = 7A_g + 5B_{1g} + 7B_{2g} + 5B_{3g} \ldots\ldots\ldots\ldots\ldots\ldots\ldots\ldots (1)$$

Equation (1) shows the 24 Raman active modes possible for *Pnma* symmetry. Structural distortions in pervoskites are generally attributed to atomic phenomena which include rotation of CrO_6 octahedra, displacement of cations and Jahn-Teller (JT) distortion[35].In the present studies the structural distortions are expected to happen either by the rotation of CrO_6 octahedra and/or A-site displacement of cations whereas inactive Jahn-Teller ion (Cr^{3+}) cannot create any distortions within the unit cell. It is known that change in bond angles, bond lengths and tilt angles of the CrO_6 octahedra are decisive of functional properties of chromites [22, 25]. The Raman spectra of NBiCO captured at RT is shown in Fig 2 and the Raman mode assignments (shown in Table 2) were performed in accordance to orthochromites[34,35,36]. In order to identify the Raman shift peaks for different 'Bi' substituted samples, the NBiCO Raman spectra were fitted in the range of 100-600 cm^{-1} by a Gaussian profile [30] and each of the profile is characterized by three parameters namely frequency shift, intensity and line width. We observed 14 Raman modes out of 24 possible modes for *Pnma* structure. As we increase the substitution noticeable change in the phonon modes like A_g (5), B_{3g} (5), A_g (6), B_{2g} (6) and B_{3g} (2) shift to red frequency regime. The peak position depends on the natural vibrational frequency of the isolated molecule and the interactions with the environment. It is known that heavier atoms occupying at the A-site vibrates at low frequencies and that of light atoms like oxygen vibrate at relatively higher frequencies based on the relation $\nu \alpha (K/\mu)^{1/2}$ where K force constant depends on the interaction strength between atoms, ν the frequency and μ is the reduced mass[14]. Due to similar ionic radius of Bismuth the relative shift to red frequency observed in the Raman modes like A_g (6), A_g (5), B_{3g} (5) could be due to the heavier ion of Bi in Nd-site .The relatively heavier Bi cation could potentially alter the interactions among Nd-O modes and eventually resulting in observed shift of B_{2g} (6) ($5cm^{-1}$) and B_{3g} (2) ($21cm^{-1}$) with 'Bi'composition and such significant changes observed in these phonon modes could be due to the weakening of interactions among A/B-site cation with oxygen atom and/or oxygen stretching modes with substitution. Thus the Nd-O bond lengths observed from the XRD measurements are minor but its effect is dominantly visible in our Raman studies. The octahedral rotations of CrO_6 as observed in B_{1g} (3) and B_{3g} (3) which shifts in blue frequency regime i.e. increases the strength of interaction with Bismuth composition. Thus Bi substitution can create the short range forces which lead to increasing the force constant and vibrational frequencies, become more effective with composition [37]. The

interaction strength can only be observed when the bond distances/lengths are coming closer with substitution. This can be seen from the minor decrease of Cr-O2 bond lengths and change in bond angles along Cr-O2-Cr.The three modes A_g (2), A_g (4) and B_{1g} (3) are observed as individual modes in NCO, whereas with substitution of Bi they merge to a single broader phonon mode. The broader phonon mode was deconvoluted into three modes (~ 280-370cm^{-1}) and shown in Fig 2 resulting from atomic motions related to A-cation and CrO_6 out of phase x-rotations. The variation of line widths (full width half maximum, FWHM) of three modes is shown in Fig 3 and it shows that the FWHM are related to the environmentally induced frequency fluctuations due to electrostatic forces or inherent disorder leads to increase of broadening with Bismuth [37,38]. In addition we observe a unique Raman mode at B_{2g} (2) (Octahedral tilt, refer Table 2) with an enhanced Raman intensity as composition increases, which might arise from the oxygen sublattice. The increased intensity of B_{2g} (2) with composition reveals that the structural distortions introduced in NCO could be due to oxygen stretching modes at higher wavenumbers. The major changes observed in Raman modes with Bismuth substitution suggests that the change rotational and/or CrO_6 bending, Nd-displacement and oxygen stretching could collectively create the distortions observed. The structural distortions could arise from the octahedral site rotations plausibly arising from changes in the Cr-O and Nd-O bonds However, these structural distortions on an average scale i.e. from XRD measurements are minor the effects could be dominantly seen in Raman scattering experiments.

3.3 Magnetic properties

The magnetic molar susceptibility (χ_m) as a function of temperature (T) from 5 to 300K in magnetic field of 100Oe is plotted for zero field cooling (ZFC) and field cooled (FC) conditions (Fig 4(a)). With falling temperature, the first magnetic ordering (Neel Transition Temperature, T_N was obtained by using the derivative plots of Magnetization as seen from the inset of Fig 4(b)) was observed at 230K for NCO which is attributed to cooperative Cr^{+3} spin ordering. It is found that T_N decreases linearly from 230(x=0) to 223K (x=0.1). The Cr sublattice undergoes a long range cooperative ordering transition that can be observed in drop of magnetization (around Neel Transition) in χ_m-T measurements in NBiCO samples. Below T_N the spontaneous magnetization first increases with decreasing temperature, reaching a maximum around T=187K. It then decreases and exhibits a

minimum around T=100K, below which it again increases to a maximum at 35 K(x=0). The unusual temperature dependence of magnetic behaviour can be explained by strong effective field on the Nd^{3+} moments by the ordered Cr^{3+} spin system [11]. Thus below T_N the Cr sublattice magnetization induces an effective magnetic field on Nd sublattice due to Nd-Cr interaction which tends to polarize the system from Γ_2 (F_x, Cy, Gz) into Γ_1 (A_x, Gy, Cz) at lower temperature (related to spin reorientation; T_{SRPT}=35K for x=0) [27,39].From the Fig 4(a) ZFC curves we observed a small hump at (T~10-11K) in all the samples from x=0 to 0.1 whereas this hump is not observed in FC condition. The specific heat measurements on NCO system revealed that the hump at 10K is due to the two-level Schtokky effect caused by the split of 'Nd' ground doublet [39]. Doping Bi^{3+} into NCO increases the magnitude of χ_m below transition temperature and has a strong effect on χ_m-T behaviour below the magnetic ordering temperature. The presence of nonmagnetic Bi^{3+} in magnetic site Nd^{3+} site decreases the strength of interactions among the Nd^{3+}-Cr^{3+} leads to decrease of T_{SRPT} from 35K [x=0] to 28K [x=0.1]. To elucidate the nature of the magnetic interaction above the transition temperature T_N, inverse susceptibility has been plotted with Temperature (Fig 4(b)) following curie Weiss behaviour

$$\chi^{-1} = \frac{3k_B(T - \theta_{CW})}{N_A \mu_{eff}^2}$$

The Curie Weiss fit was done at paramagnetic region of our samples and is shown in Fig 5 for different compositions. The observed increase of effective magnetic moment values from curie fit are $5.39u_B$ (x=0) to $6.72u_B$ (x=0.1) which is greater than the theoretical calculated values of 5.29 u_B for NCO [$\mu_{eff} = [(\mu^2_{Nd3+} + \mu^2_{Cr3+})]^{1/2}$ where μ_{Nd3+} =$3.62u_B$ and μ_{Cr3+}=$3.87u_B$)]. The observed higher values of effective magnetic moment is due to curie Weiss fitting done above 250K which is immediately above the transition temperature. The higher temperature fitting i.e. 2-3 times of transition temperature may give effective moment close to Cr^{3+} values. The observed Weiss temperature (θ_{CW}), shown in Table 3, is decreases from -389 to -345K. These values signify that increase of Bi concentration strengthens the ferromagnetic interaction or weakens the antiferromagnetic interactions. Fig 6(a) & 6(b) we have shown Isothermal M-H loops at 5K and 100K for NBiCO which shows that magnetization does not saturate up to 5T. The coericivity varies from 184 Oe(x=0) to 445 Oe(x=0.1) shown in Fig 6(a) for T=5K ($T<T_{SRPT}$) (inset shows clear variation of MH loops for x=0 and 0.1) and the coericivity varies from 40Oe (x=0) to 823Oe (x=0.1) at

T=100K ($T_{SRPT}<T<T_N$) shown in Fig 6(b) (inset shows clear variation of MH loops for x=0 and 0.1). The Room temperature M-H loops (not shown here) almost straight line indicating absence of any ferromagnetic ordering above Neel Transition temperature.

It's worth remembering that the structural distortions due to the Bi substitution in NCO lattice was evident from the structural studies such as change in phonon behaviour related to CrO_6 rotations as discussed in Raman can possibly facilitate this hybridization in NBiCO samples. Chromites with Cr^{3+} configuration, only π bonds of t^3-o-t^3 are present and eventually lead to an antiferromagnetic ordering. However, in $NdCrO_3$ structures introducing a plausible *t-e* hybridsation is expected to induce an additional structural distortion in the lattice associated with a change (reduction) in the antiferromagnetic interaction. Presence of such distortion facilitates virtual charge transfer (VCT) to the empty *e* component of the hybridized orbital, i.e., t^3-O-e^0, which effectively leads to observed weak ferromagnetic coupling [22] in our compounds. Thus the present study Bi with similar ionic radii, but with a $6s^2$ lone pair configuration plausibly create the local structural distortions due to rotations of CrO_6 further leads to *t-e* hybridization which in turn changes the values of T_N in our chromites. The observed increase of 40 Oe to 830Oe above T_{SRPT} and 184 Oe(x=0) to 445 Oe(x=0.1) below T_{SRPT} gives a clear indication that Bi^{3+} can influence greater in Cr^{3+}-Cr^{3+} interaction than that of Nd^{3+}-Cr^{3+} interaction. Thus nonmagnetic Bi^{3+} alter the magnetic interactions of Nd^{3+} and Cr^{+3} ion coupling which can be observe as change in T_{SRPT} (ΔT~7K with composition) .

3.4 Optical Studies

Bi^{3+} cation is expected to interact strongly with the Cr - oxygen interaction and hence the optical absorption features of NCO would be strongly influenced by Bi substitution. Hence, the optical absorption studies were carried out to study the influence on optical band gap of NCO with Bi substitution. The optical absorption edge was analyzed by the following relation ship

$$\alpha h\nu = A(h\nu - E_g)^m$$

Where A is constant, m value is ½ and 2 for direct and indirect transitions respectively and E_g is the optical band gap [40]. The optical absorption spectrum of Cr^{3+} ion in NBiCO was recorded at room temperature (RT) from λ=200nm

to 900nm. The absorption spectrum of NBiCO is typical of Cr^{3+} in a predominantly octahedral environment. The value of optical band gap was estimated from the linear fitting and extrapolation of the $(\alpha hv)^2$ vs. *hv* graph to the *hv* axis band gap of the compounds as shown in Fig 7 and inset shows the absorption spectrum plotted with wavenumber. The studies reveal that the NCO ceramics have a direct band gap characteristics and the absorption edge is observed at 3.1eV for NCO. The absorption edge of NCO is primarily associated with the manifold of Charge transfer transitions between O (2p) and Cr (3d) states [41] and this value decreases to 2.6 eV from 3.1 eV with increase of Bi content in NCO. The other optical absorption bands commonly observed in ortho chromites arising from *d-d* transitions of Cr^{3+} were also present. The optical absorption from ground state (electronic configuration of Cr^{3+} ion) $^4A_2$ to $^4T_2$ and $^4T_1$ leads to observed two intense and broad bands were recorded at 16863cm^{-1} and 21645cm^{-1}. In addition to that two sharp bands at lower energies due to optical absorption from $^4A_2$ to $^2T_1$ and ^2E_g at 13377 $cm^{-1}$and 12446 $cm^{-1}$for NCO was also observed. The variation of optical absorption edge evidently suggests that Bi ($6s^2$) substituted in the magnetic rare earth Nd^{+3} influences the Cr-O overlap integral. This increase of interaction of Bi cation with oxygen bonds influences the structural distortions through Cr-O polyhedra [42]. Thus the changes in rotational octahedra distortions observed through Raman scattering measurements and Cr-O changes through optical studies are in good agreement and this distortions that could plausibly be responsible for the observed changes in Neel transition temperatures as well as ferromagnetic nature in these compounds. Hence, the tunable optical properties such as bandgap from 3.1 to 2.6eV and enhanced weak ferromagnetism (40 Oe to 830Oe) associated with structural distortions in NBiCO could be used for photocatalytic and magnetic applications [43,44].

4. CONCLUSIONS:

$Nd_{1-x}Bi_xCrO_3$ ceramics with 'x' varying from 0 to 0.1 at% were successfully synthesized through Sol-gel method. All the compositions studied and they are stabilized in an orthorhombic *Pnma* structure, which was evident from the refinement studies. The variation of optical absorption edge evidently suggests that Bi ($6s^2$) substituted in the magnetic rare earth Nd^{+3} influences the Cr-O overlap integral. This increase of interaction of Bi cation with oxygen bonds influences the structural distortions through Cr-O polyhedra were evident from the Raman studies.

Nonmagnetic and similar ionic radius of Bi^{+3} in Nd^{+3} creates local structural distortions due to plausible nature of $6s^2$ electron configuration of Bi^{+3}. These structural distortions further influence the magnetic properties in our present studied samples. The involvement of *t-e* hybridization along with canting angle of Cr-O-Cr leads to the observed change in T_N from 230 to 223K and T_{SRPT} from 35 to 28K with Bi^{+3} content. Isothermal magnetization curves performed at 100K ($T>T_{SRPT}$) shows increase of coercive field from 40 to 830Oe gives clear evidence of Bi^{3+} can influence Cr^{+3}-Cr^{+3} exchange interactions.

ACKNOWLEDGEMENTS

Authors V.R.Mannepalli and R.R would like to acknowledge DST, India, and No.SERB/F/5142/2013-14/ for financial support to carry out the research.

Table 1 Refinement details of $Nd_{1-x}Bi_xCrO_3$(x=0, 0.05 and 0.1) for orthorhombic *Pnma* space group

Refined Parameters		X=0	X=0.05	X=0.1
a (Å)		5.4849(6)	5.4838(7)	5.4885(4)
b (Å)		7.6936(7)	7.6930(8)	7.6989(6)
c (Å)		5.4197(6)	5.4180(7)	5.4214(4)
Cr-O1		1.984(8)	1.986(9)	1.973(8)
Cr-O2		1.97(2)	1.95(3)	1.95(3)
		1.99(2)	2.01(3)	2.03(3)
Cr-O1-Cr		151.5(3)	151.1(4)	154.5(3)
Cr-O2-Cr		154.3(9)	154.2(11)	152.3(12)
Bragg R-Factor (R_B)		6.54	11.6	15.5
RF-factor		5.76	9.57	13.4
χ^2		1.21	1.52	1.52
R_p		9.08	7.23	7.0
R_{wp}		11.8	9.40	9.03
R_{exp}		10.75	7.62	7.31
Thermal parameter (B)(Å^2)		1.48	2.22	2.11
Volume(Å^3)		228.7	228.6	229.1
Composition	**Positions→ / Ions↓**	**x**	**y**	**z**
X=0	Nd^{3+}/Bi^{3+} 4(c)	0.0414(3)	0.25	0.0084(7)
	Cr^{3+} 4(b)	0	0	0.5
	O1 4(c)	0.477(4)	0.25	-0.087(6)
	O2 8(d)	0.296(4)	0.035(4)	-0.294(4)
X=0.05	Nd^{3+}/Bi^{3+} 4(c)	0.0403(4)	0.25	0.0056(9)
	Cr^{3+} 4(b)	0	0	0.5
	O1 4(c)	0.462(4)	0.25	-0.083(7)
	O2 8(d)	0.289(5)	0.045(4)	-0.282(5)
X=0.1	Nd^{3+}/Bi^{3+} 4(c)	0.0413(4)	0.25	0.0055(10)
	Cr^{3+} 4(b)	0	0	0.5
	O1 4(c)	0.463(5)	0.25	-0.071(7)
	O2 8(d)	0.281(5)	0.056(3)	-0.271(6)

Table 2 Raman modes at Room temperature for $Nd_{1-x}Bi_xCrO_3$

Assignment of modes	X=0	X=0.05	X=0.1	Activating distortion	Atomic motions
$A_g(7)$	142	143	140	A-shift	
$A_g(5)$	151	149	142	rot[010]	A(x)
$A_g(6)$	195	195	181	rot[101]	CrO_6 in phase y rotations
$B_{3g}(5)$	168	165	161	rot[101]	
$B_{2g}(6)$	211	211	206	A-shift	A(Z),O1(Z),
$A_g(2)$	288	288	286	rot[010]	O1(x),A(-x)
$A_g(4)$	332	331	330	rot[101]	A(Z),O1(-Z),
$B_{1g}(3)$	367	379	386	rot[101]	CrO_6 out of phase x rotations
$B_{3g}(3)$	434	438	439	rot[101]	Out of phase O2 scissors like
$A_g(1)$	452	452	449	rot[010]	CrO_6 bendings
$B_{2g}(2)$	--	513	504	rot[010]	
$B_{1g}(2)$	551	551	550	rot[101]	CrO_6 out of phase Bendings
$B_{3g}(2)$	575	569	554	rot[101]	O2,O1 antistrecthing

Table 3 Coercive fields, Weiss temperature and Neel Transition temperatures for different compositions.

	X=0	**X=0.05**	**X=0.1**
H_c(Oe) at 5K	184	450	445
H_c(Oe) at 100K	40	175	823
Neel Temperature (K)	230	228	223
Weiss Temperature (K)	-389	-350	-345

REFERENCE

[1] Joseph Sfeir, J.Power Sources **118** (2003) 276-285.

[2] Minh N.Q, J. Am. Ceram. Soc **76** (1993) 563-588.

[3] A.Ngueteu kamlo, J.Bernard, C.lelievre, D.Houivet, J. Eur. Ceram. Soc. **31**(2011) 1457-1463.

[4] B. Rajeswaran, D. I. Khomskii, A. K. Zvezdin, C. N. R. Rao, and A. Sundaresan, Phys. Rev. B **86** (2012) 214409 (1-5).

[5] M.El Amrani, M.Zaghrioui, V. Ta Phuoc, F.Gervais, Nestor E. Massa, J.Mag.Magn.Mater **361**(2014)1-6.

[6] C.R.Serrao, A.K.Kundu, S.B.Krupanidhi, U.V.Waghmore and C.N.R Rao, Phys. Rev. B **72**(2005) 220101(R) (1-4).

[7] J.-D Seo, J.Y.Son, J Cryst Growth **375** (2013) 53-56.

[8] K. Ramesha, A Llobet, Th. Proffen, C. R. Serrao, and C. N. R. Rao, J. Phys. Condens. Matter. **19**(2007) 102202 (1-8).

[9] Yogesh Sharma, Satyaprakash Sahoo, William Perez, Somdutta Mukherjee, Rajeev Gupta, Ashish Garg, Ratnamala Chatterjee, and Ram. S. Katiyar, J. Appl. Phys. **115**(2014)183907(1-9).

[10] Nirat Ray and Umesh V.Waghmare, Phys. Rev. B **77**(2008) 134112 (1-10).

[11] R.M.Hornreich, J.Mag.Magn.Mater **7**(1978) 280-285.

[12] N. Shamir, H. Shaked and S. Shtrikman, Phys. Rev. B **24**(1981) 6642-6651.

[13] K.Sardar, M.R. Lees, R.J.Kashtiban, J.Sloan and R.I.Walton, Chem Mater **23** (2011) 48-56.

[14] L M Daniels, M.C.Weber, M.R.Lees, M.Guennou, R.J. Kashtiban, J.Sloan, J.Kreisel and R.I Walton, Inorg Chem **52**(2013) 12161-12169.

[15] Kenji Yoshii, Mater Res Bull **47** (2012) 3243-3248.

[16] Y.Su, J.Zhang, L Li, B Li,Y Zhou, D Deng, Z Chen and S Cao, Appl Phys A **100** (2010) 73-78

[17] G.G.Artem'ev, A.M.Kadomtseva, V.N.Milov, M.M Lukina, A.A.Mukhin, J Mag Mag Mater **140-144**(1995) 2157-2158.

[18] R M Horneriech, Y.Komet and B.M Wanklyn, Solid State Commun **11**(1972) 969-972

[19] Y.Su, J Zhang, Z Feng, L Li, B Li, Y Zhou, Z Chen and S Cao, J Appl Phys **108** (2010) 013905 (1-6)

[20] A H Cooke, DM Martin and MR Wells, J.Phys.C: Solid state Phys **7**(1974) 3133-3144.

[21] D.Treves, M.Eibschutz and P.Coppens, Phys.Lett. **18** (1965) 216-217

[22] J. S. Zhou, J. A. Alonso, V. Pomjakushin, J. B. Goodenough, Y. Ren, J. Q. Yan, and J. G. Cheng, Phys. Rev. B **81**(2010) 214115(1-5).

[23] J.D.Dunitz and L.E.Orgel. J.Phys.Chem.Solids **3** (1957) 20-29.

[24] Shan Wang, Keke Huang, Changmin Hou, Long Yuan, Xiaofeng Wu and Dayong Lu, Dalton Trans. **44** (2015) 17201-17208.

[25] J. S.Zhou and J. B. Goodenough. PRL **96** (2006) 247202 (1-4) and Phys. Rev. B **77** (2008) 132104(1-4)

[26] Michael W Lufaso, Samuel J Mugavero, William R Gemmill, Yongjae Lee, Thomas Vogt, Hans-Conrad zur Loye, J Alloys Compounds **433** (2007) 91-96.

[27] R.M.Hornreich, Y.Komet, R.Nolan, B.M. Wanklyn, and I.Yaeger. Phys. Rev. B **12** (1975) 5094-5104.

[28] K.R Chakraborty, S.Mukherjee, S.D Kaushik, S.Rayaprol, C.L.Prajapat, M.R.Singh, V.Siruguri, A.K.Tyagi and S.M.Yusuf, J Magn Magn Mater **361**(2014) 81-87.

[29] H.Satoh, S Koseki, M Takagi, W Y Chung, N Kamegashira. J Alloy and Compd **259** (1997) 176-182.

[30] Yi Du, Zhen Xiang Cheng, Xiao-Lin Wang and Shi Xue Dou. J.Appl.Phys **108** (2010) 093914 (1-9)

[31] J. B. Neaton, C. Ederer, U. V Waghmare, N. A. Spaldin, and K. M. Rabe, Phys. Rev. B **71**(2005) 014113(1-8).

[32] S.Niitaka, M.Azuma, M.Takano, E.Nishibori, M.Takata, M.Sakata Solid State Ionics **172**(2004) 557-559.

[33] J.Rodrigues-Carvajal, An introduction to the program Fullprof Rietveld Refinement and Pattern matching Analysis. Laboratoire Leon Brillioun CEA-CNRS, France (2000)

[34] M.V. Abrashev, J. Bäckström, L. Börjesson, V.N. Popov, R.A Chakalov, N. Kolev, R.-L. Meng, and M. Iliev Phys. Rev. B **65** (2002)184301(1-9).

[35] M. C. Weber, J. Kreisel, P. A. Thomas, M. Newton, K. Sardar, and R. I. Walton Phys. Rev. B **85** (2012) 054303(1-9)

[36] N. D. Todorov, M. V. Abrashev, V. G. Ivanov, G. G. Tsutsumanova, V. Marinova, Y.-Q. Wang, and M. N. Iliev. Phys. Rev. B **83** (2011) 224303(1-6).

[37] Wolfgang Schindler and Jiri Jonas J.Chem.Phys **72** (1980) 5019-5025.

[38] Kenneth S.Schweizer and David Chandler. J.Chem.Phys **76** (1982) 2296-2314.

[39] F. Bartolomé, J. Bartolome, M. Castro, and J. J. Melero. Phys. Rev. B **62** (2000) 1058-1066.

[40] Feng Gu, Shu Fen wang, Meng KaiLu, Guang Jun Zhou, Dong Xu and Duo Rong Yuan J.Phys.Chem.B. **108**, (2004) 8119.

[41] A.V.Zenkov Research Letters in Physics 2008 Article ID 749305 (doi:10.1155/2008/749305)

[42] A.K.Tripathi and H.B.Lal Mat.Res.Bull **15** (1980) 233.

[43] Rakesh Shukla, Jayappa Manjanna, Anup K.Bera, Seikh M. Yusuf and Avesh K. Tyagi Inorganic chemistry 48, (2009) 11692-11696

[44]Rakesh Shukla, Anup K. Bera, Seikh M. Yusuf, Sudhanshu K. Deshpande, Avesh K. Tyagi, Wilfried Hermes, Matthias Eul, and Rainer Po¨ttgen J. Phys. Chem. C 113, (2009)12663–12668.

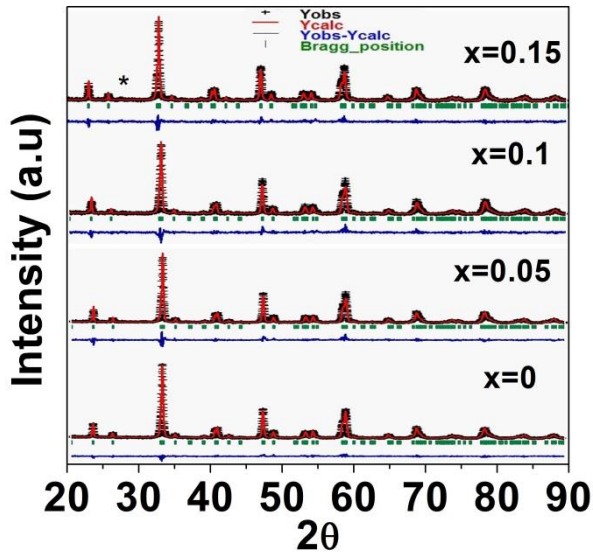

Fig 1 (color online) represents the XRD patterns at Room temperature for compositions x=0 to x=0.15 in $Nd_{1-x}Bi_xCrO_3$. * indicates the minor impurity of Bi_2O_3

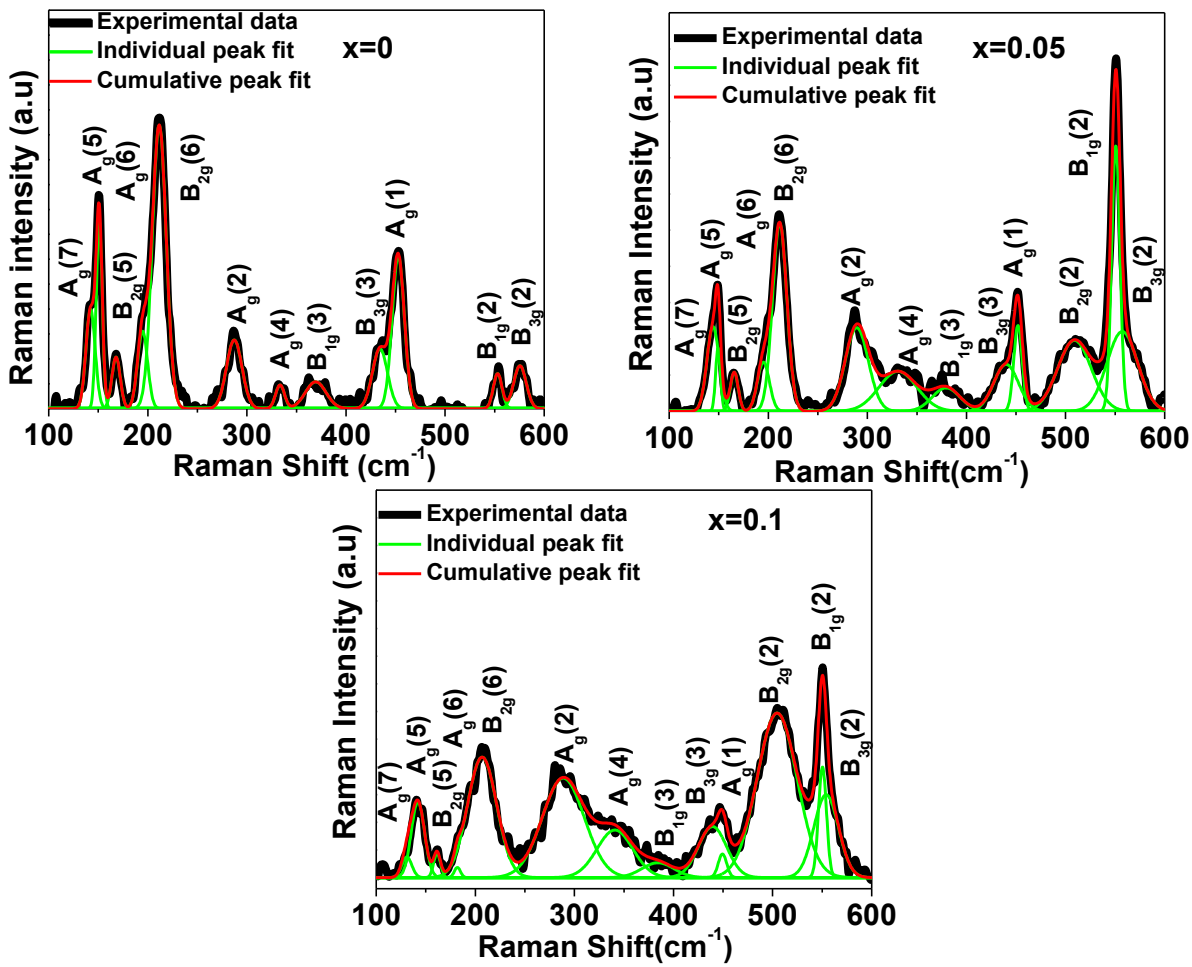

Fig 2 (color online) The Raman studies on $Nd_{1-x}Bi_xCrO_3$ (x=0 to 0.1) compound at room temperature. The Raman modes are fitted with Gaussian profile method from 100-600cm^{-1}.

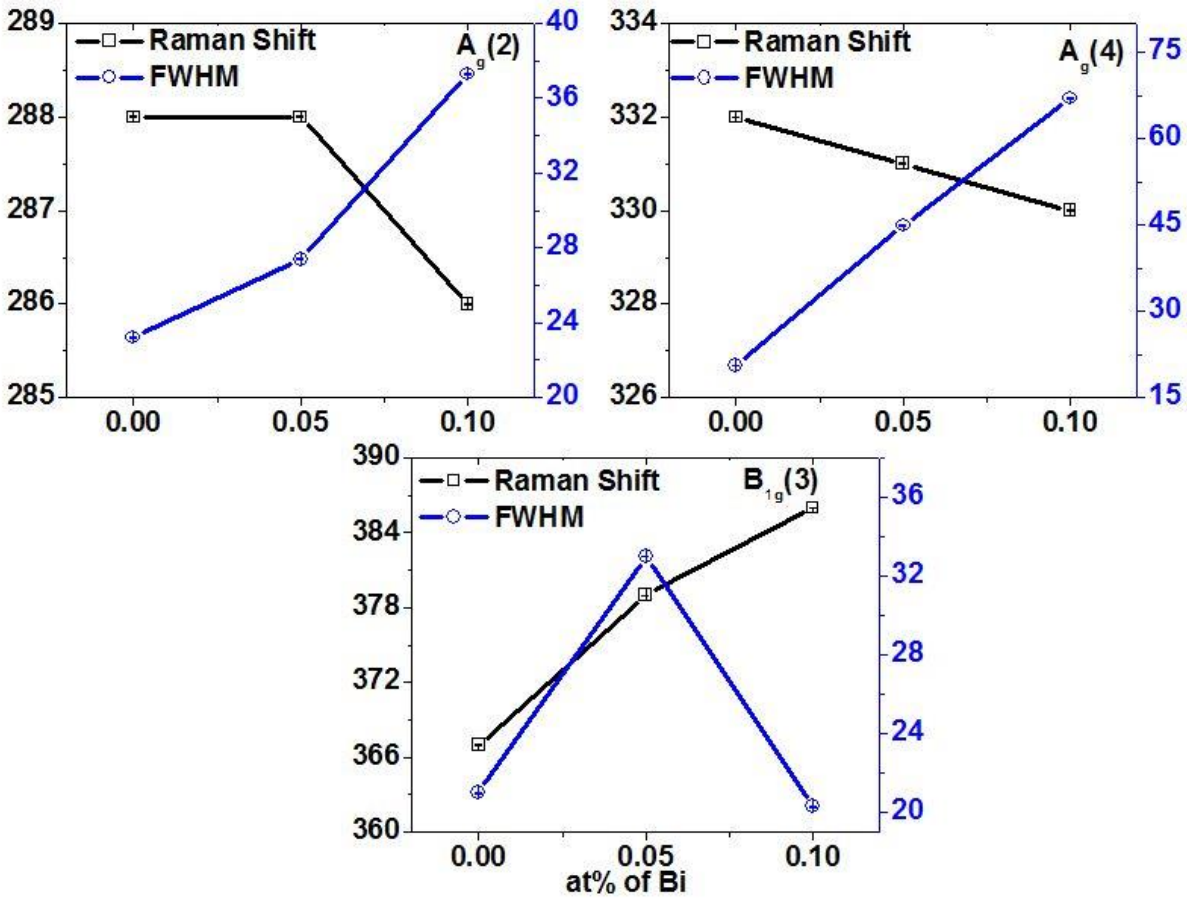

Fig 3 (color online) Raman shift and FWHM variation of A_g (2), A_g (4) and B_{1g} (3) with composition.

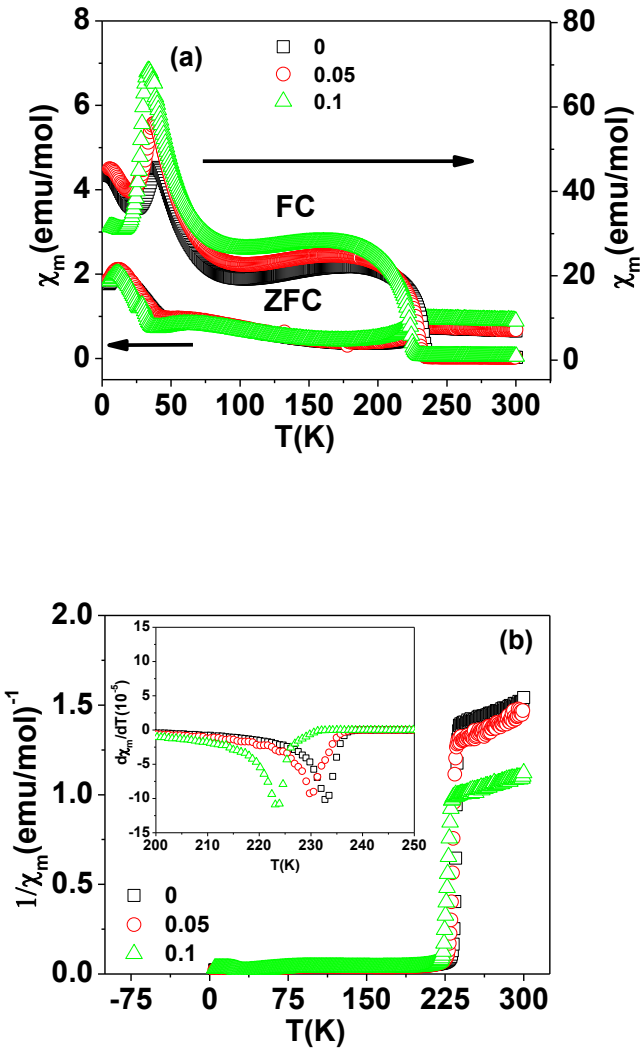

Fig 4 (color online) the magnetic studies on $Nd_{1-x}Bi_xCrO_3$ a) ZFC and FC done under the application of 100Oe magnetic field and b) inverse susceptibility with temperature (inset shows Neel transition temperatures obtained from the derivative plots)

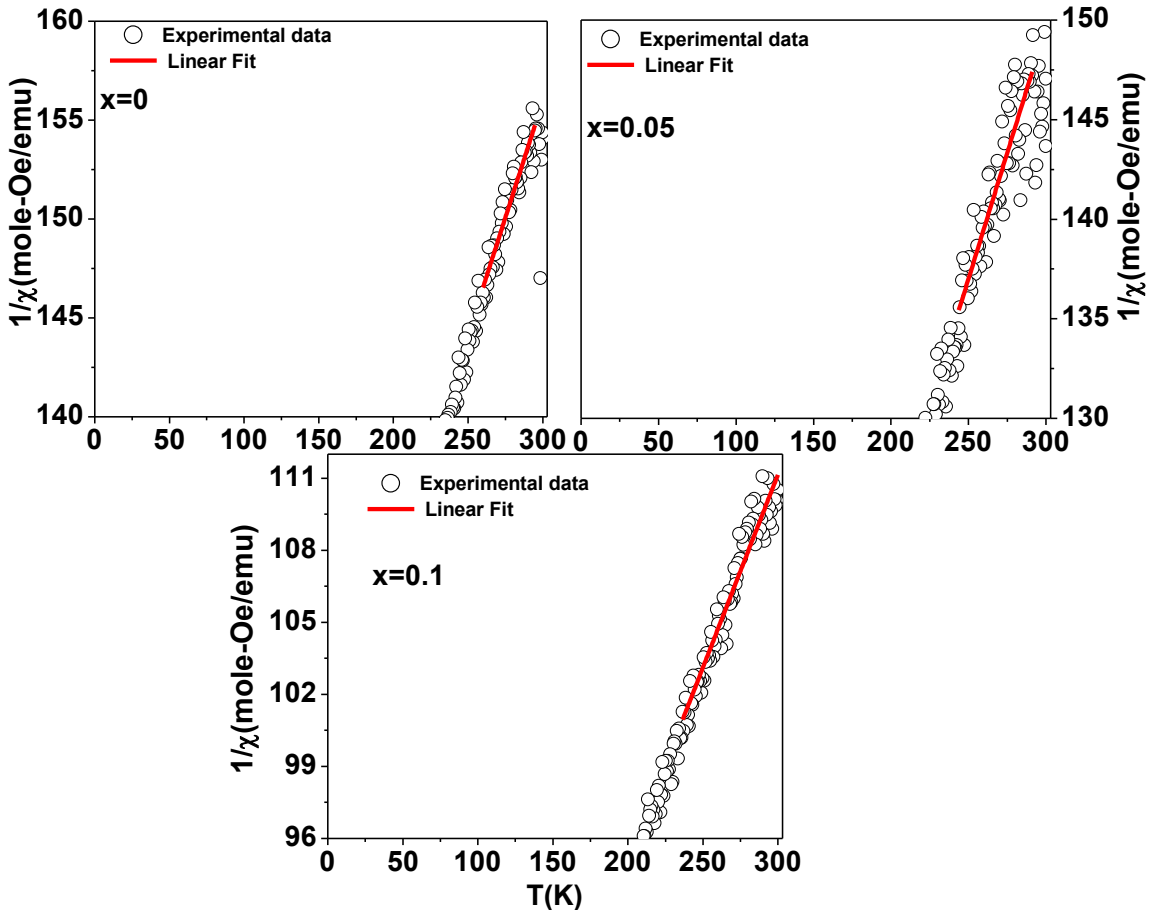

Fig 5 Curie-Weiss fitting from inverse susceptibility with temperature for different compositions

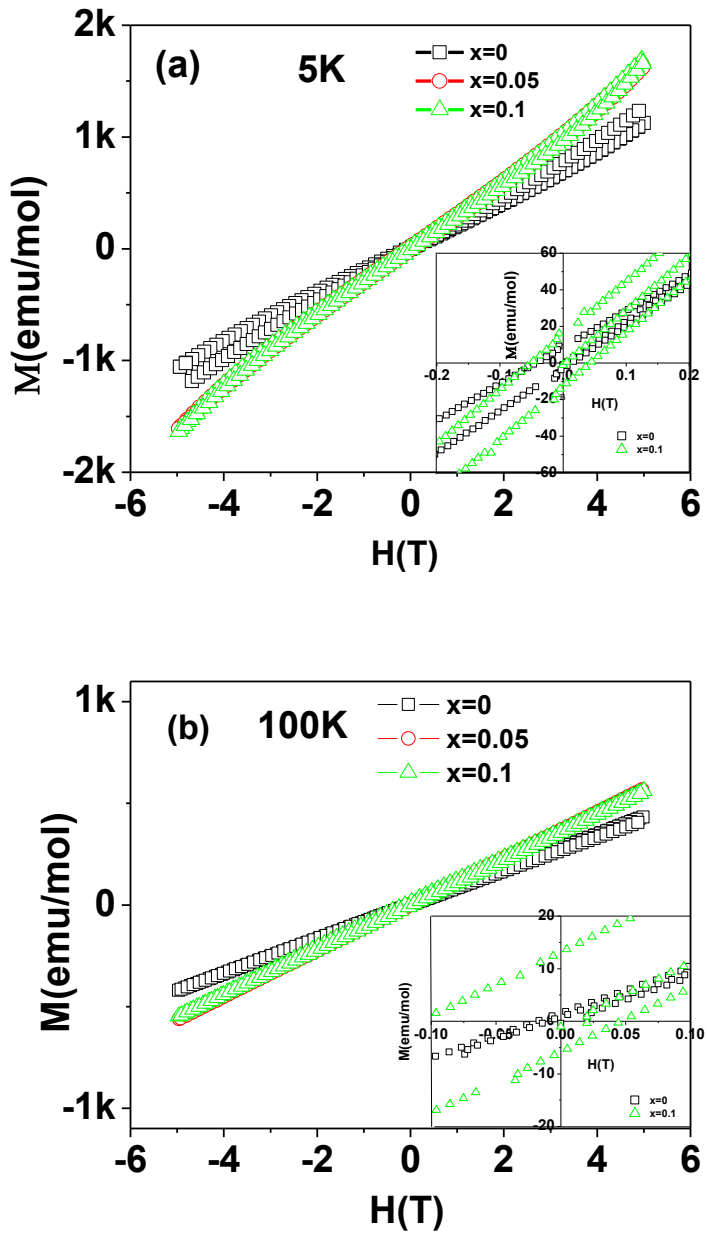

Fig 6 (color online) Isothermal MH-plots upto 5Tesla at a) 5K and b) 100K for different compositions of Bismuth. Inset shows zoom portion of MH loops for x=0 and 0.1 at 5K and 100K

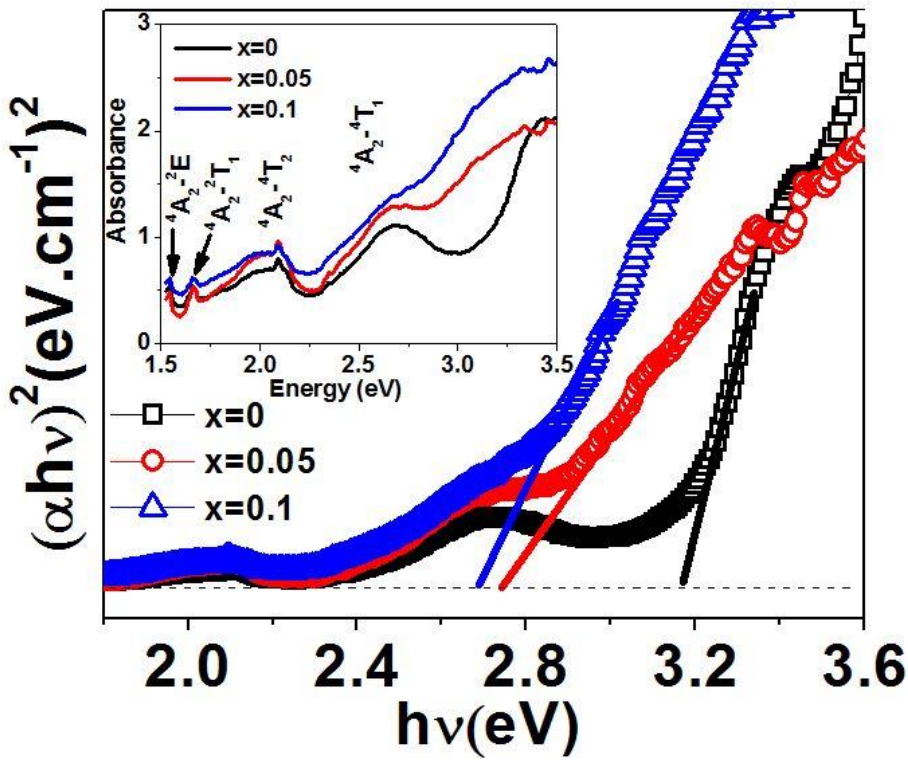

Fig 7. UV studies for calculation of Band gap NBiCO (x=0 to 0.1).inset shows optical absorption bands related to *d-d* transitions